Simulation of Tool Rotation and Travelling Speed Effects on Friction Stir Welding of Ti-6Al-4V

Hamed Aghajani Derazkola[1*]
[1]Young Researchers and Elites club, Science and Research Branch, Islamic Azad University, Tehran, Iran
[*]Email of Corresponding Author: h.aghajany@gmail.com
Received:September 30, 2019; Accepted: December 24, 2019

Abstract
In this research, the effects of parameters include tool rotational and traverse speeds were investigated on heat generation and material flow during friction stir welding of Ti-6Al-4V alloy with computational fluid dynamics (CFD) method. Simulation results showed that with increasing of tool rotational and decreasing tool traverse speed, the more frictional heat generates which causes formation of bigger stir zone. Results indicate that the rotation of the shoulder can accelerate the material flow behavior near the top surface. The temperature field in the friction stir welding of Ti-6Al-4V alloy was anti symmetric to the welding line. Due to the results the heat generation and temperature distribution at advancing side were more than retreating side in all joint conditions. According to the results unsmooth and disarray flow patterns were formed in stir zone which caused formation of banded layer structure in advancing side. Due to results the torque decreases with an increase in the tool rotation speed due to increases in the heat generation rate and temperature, but torque is not significantly affected by the change in welding speed. The computed pressure field was higher in front of the tool compared to the trailing edge, and it is because pressure difference is required for flow occur. According to the selected parameters in this study, maximum temperature was produced in 800rpm tool speed and the computed strain rate and pressure of workpiece in this speed were 2.3 s^{-1}, 0635 MPa, respectively.

Keywords
Friction Stir Welding, Ti-6Al-4V Titanium Alloy, Computational Fluid Dynamic, Thermal Modeling.

1. Introduction
Ti-6Al-4V titanium alloy is extensively used in aero, marine, energy and biomedical industries due to good mechanical and chemical properties. Manufacturing of the titanium structures often requires welding process, which is typically achieved by conventional fusion welding techniques. However, formation of brittle solidification microstructures, large distortions, and significant residual stresses may limit the use of the conventional joining methods. In some circumstances, utilization of a solid-state joining approach is desirable and friction-stir welding (FSW) is one of the possible candidates [1-2]. In this method a non-consumable rotating tool with a pin is plunged into the joint arbitrary line between raw materials. The FSW tool is producing local heat with frictional contact and plastic deformation of base material. The hot material is forced to flow around the rotating probe to fill the cavity at the rear of the moving tool, thus form a weld in a solid state [3-4]. The combination of the rotation and traverse motions of the tool creates a characteristic asymmetry of FSW: the advancing side, where the direction of the tool rotation is the same as that of the tool translation, and the

retreating side, where they are opposite [5]. During FSW process, the material which undergoes extreme levels of strain rates and thermal exposure, normally leads to the drastic micro structural changes [6]. Currently, FSW is well-proven to be a highly efficient joining technique, enabling the production of high quality welds with excellent service properties, thus having great industrial potential [7-8]. However, due to the high requirements to the welding tools, FSW of titanium alloys is relatively difficult, and, until recently, work in this area has been limited [9]. With the aim of providing a useful guide in this area, this study attempts to summarize the simulation process of FSW of Ti-6Al-4V to find better understanding behavior of this material during solid state joining process.

To better understand these factors and the development of models, many researchers worked to simulate the process by computational fluid dynamic (CFD) technique. Researchers such as Smith [10] and North [11] were among the first researchers that used the CFD to simulate FSW process. They were modeled the workpieces as non-Newtonian fluid in their simulations. Seidel and Reynolds [12] present a two-dimensional model to predict material flow in friction stir welding. They observed that at the low rotational and linear speed the composition of the fluids occurs substantially horizontally. This effect indicates the need for further analysis of process in 3D. Zhang et.al [13] with development of the 2D material flow concluded that the material behind tool had largest deformation compared to the other parts around the pin. This angular deformation occurs between 300 to 360 degrees. Material flow during FSW of carbon steel with the use of 3D CFD model was investigated by Nandan et. al. [14-15]. They were solved the process based on momentum, energy and mass transfer equations. Nandan et. al. defined non-Newtonian fluid for simulation and predicted the viscosity, strain rate, temperature and stir zone of carbon steel during friction stir welding. Nassar et. al [16] studied on FSW of AZ31B Mg according to Eulerian model and the heat transfer problems. They concluded that by increasing the rotational speed, the weld zone temperature rises and with increasing linear speed it decreases. Ji et. al [17] studied the effect of the FSW tool pin profile on the material flow. By developing CFD modelling of FSW process, some researches were done on dissimilar joint simulation. Recently Aghajani derazkola and Simchi [18], and Elyasi and Aghajani derazkola [19] developed CFD code by viscosity shear rate model for FSW simulation of PMMA polymer. Computational fluid dynamics (CFD) model for dissimilar joint of AA6061-AA5083 and AA2024-AA7075 aluminum alloys were investigated by Kishor et al. [20]. By study on heat generation and material flow for the three different pin profiles and different positions of materials, they finally showed that the peak temperature was generated at the harder material. Padmanaban et al. [21] used a CFD model as well as VOF model for studying heat transfer and material flow of AA2024 and AA7075 dissimilar joint. Liu et al. [22] used a coupled thermo-mechanical model to study the dissimilar FSW of 6061 Al alloy to TRIP steel. Their results showed that considering a frictional shear stress contact condition made a much more better material distribution than the velocity contact condition. Aghajani derazkola et al. [23] reported the results of a three dimensional heat generation simulation based on CFD during FSW of AA1100 aluminum alloy and AISI A441 steel. They defined two volumetric heat equations. One of these equations defined the heat generated at the interface of the tool pin and the workpiece and the other equation was used for the heat generated from the viscous dissipation. The equation of viscous heating is used in this work. Aghajani derazkola et al. [24] used this model for simulation between

Al-Mg alloy and PMMA polymer at another investigation. JamshidiAval et al. [25] made a 3D thermal model based on finite element method (FEM) for dissimilar joint of AA5086 and AA6061 aluminum alloys. Their results showed the asymmetric heat generation that agreed with simulations based on CFD.

The purpose of this article is investigation on the effects of FSW tool travelling and rotational speed on the frictional heat generation, temperature distribution and cooling rate of Ti-6Al-4V titanium alloy based on the developed previous models. This research was done based on previous model development and their relation to chemical diffusion equation with plastic deformation of Ti-6Al-4V titanium alloy during FSW with tungsten tool.

2. Process Modeling

2.1 Governing Equations

The computational domain in this study includes the workpiece and the tool inserted inside the workpiece. The dimensions of the plate and the tool used and the properties of the workpiece and the tool material are given in Table 1. During the simulation tool plunge stage and extraction from the joint line are neglected for simplicity. Therefore, the temperature and velocity fields are solved assuming steady state behavior. The plastic flow in a three dimensional is represented by the momentum conservation equation in index notation, with i or j = 1, 2 and 3, representing x, y and z directions, respectively [24]:

$$\rho \frac{\partial u_i u_j}{\partial x_i} = -\frac{\partial P}{\partial x_j} + \frac{\partial}{\partial x_i}\left(\mu \frac{\partial u_i}{\partial x_j} + \mu \frac{\partial u_j}{\partial x_i} \right) - \rho U_1 \frac{\partial u_j}{\partial x_1} \tag{1}$$

In Equation (1), u is the velocity, ρ is the density, U1 is the welding velocity, and P is the pressure and μ is refer to non-Newtonian viscosity that can be determined from flow stress and effective strain rate as follows [24]:

$$\mu = \frac{\sigma_e}{3\dot{\varepsilon}} \tag{2}$$

The calculation of viscosity requires local value of strain rate and temperature. In Equation (2), σ_e indicated the flow stress that proposed by Sheppard and Wright [24]:

$$\sigma_e = \frac{1}{\alpha} arc\sinh\left(\frac{Z}{A}\right)^{\frac{1}{n}} \tag{3}$$

Where A, a, and n are material constants and Z is the Zener–Hollomon parameter. The value of constants for AA1100 aluminum alloy are A = 3.51 *10^{10} S^{-1}, a=1 MPa^{-1}, and n=5.66 [17]. The Zener–Hollomon parameter, Z, represents the temperature compensated effective strain rate and is given by [23]:

$$Z = \dot{\varepsilon} exp^{\left(\frac{Q}{RT}\right)} \tag{4}$$

Where, Q=158.3kJ/mol [19] is the temperature-independent activation energy, R is the universal gas constant, $\dot{\varepsilon}$ is the effective strain rate and given by [23]:

$$\dot{\varepsilon} = \sqrt{\left(\frac{2}{3}\varepsilon_{ij}\varepsilon_{ij}\right)} \tag{5}$$

Where, ε_{ij} is the strain rate tensor, defined as [23]:

$$\varepsilon_{ij} = \frac{1}{2}\left(\frac{\partial u_i}{\partial x_j} + \frac{\partial u_j}{\partial x_i}\right) \tag{6}$$

According to the materials physical changes during hot working, achieve the relation with mechanical and thermal properties during FSW in simulation procedure is necessary. Based on this factor, the Ti-6Al-4V alloy C_P and K parameters are defined as [26]:

$$C_p = 622 - 0.367T + 5.54\times10^{-4}T^2 + 2.39\times10^{-8}T^3 \tag{7}$$

$$K = 19.2 + 0.189T - 1.53\times10^{-5}T^2 - 1.41\times10^{-8}T^3 \tag{8}$$

Similarly for Tungsten [27]:

$$C_p = 158 - 0.106T - 1.63\times10^{-5}T^2 \tag{9}$$

$$K = 0.367 - 2.29\times10^{-4}T + 1.25\times10^{-7}T^2 \tag{10}$$

The pressure field was obtained by solving the following continuity equation iteratively with the momentum equations for incompressible single phase flow [23]:

$$\frac{\partial v_i}{\partial x_i} = 0 \tag{11}$$

That v_i is the velocity of plastic flow. The steady single phase momentum conservation equations with reference to a co-ordinate system attached to the heat source may be represented as [22]:

$$\rho C_p \frac{\partial\left(u_i T\right)}{\partial x_1} = -\rho C_p U_1 \frac{\partial T}{\partial x_1} + \frac{\partial}{\partial x_i}\left(k\frac{\partial T}{\partial x_i}\right) + Q_i + Q_b \tag{12}$$

The heat generated at the interface between vertical and horizontal surfaces of the tool pin and the workpiece may be defined as [22]:

$$Q_i = \left[(1-\delta)\eta\tau + \delta\mu_f P_N\right](\omega r - U_1 \sin\theta)\frac{A_r}{V} \tag{13}$$

where, A_r is any small area on the tool pin-work piece interface, r is the radial distance of the center of the area from the tool axis, V is the control volume enclosing the area A_r, s is the maximum shear stress at yielding and θ is the angle with the negative x-axis in the counter-clockwise direction, η is the mechanical efficiency (the amount of mechanical energy converted to heat energy), δ denotes the spatially variable fractional slip between the tool and the workpiece interface, lf is the spatially variable coefficient of friction, ω is the angular velocity, PN is the normal pressure on the surface. An estimate of the viscous dissipation of momentum per unit volume, Q_b, has been calculated as [23]:

$$Q_b = \frac{d\dot{\varepsilon}_p}{dV} = \beta\mu\varphi \tag{14}$$

Which, φ is given by [23]:

$$\varphi = 2\sum_{i=1}^{3}\left(\frac{\partial u_i}{\partial x_i}\right)^2 + \left(\frac{\partial u_1}{\partial x_2} + \frac{\partial u_2}{\partial x_1}\right)^2 + \left(\frac{\partial u_1}{\partial x_3} + \frac{\partial u_3}{\partial x_1}\right)^2 + \left(\frac{\partial u_3}{\partial x_2} + \frac{\partial u_2}{\partial x_3}\right)^2 \tag{15}$$

In Equation (14), β is an arbitrary constant that indicates the extent of mixing on the atomic scale. The value of μ may tend to 1for a well-mixed system in molecular scale [25]. The total heat generated at the shoulder/workpiece interface has been partitioned between the work piece and the tool in the ratio given below [22]:

$$q = \frac{\left(\sqrt{k\rho C_p}\right)_{workpiece}}{\left(\sqrt{k\rho C_p}\right)_{workpiece} + \left(\sqrt{k\rho C_p}\right)_{tool}} \tag{16}$$

Where, the subscripts W and T denote the workpiece and the tool respectively. The analytical expression is based on steady-state one dimensional heat transfer from point heat source located at the interface of dissimilar metals. The heat flux into the work piece is estimated to be 45% of the total heat generated. This relation has been examined experimentally by Lienert et al. [26] and found to be reliable. A heat flux continuity at the shoulder matrix interface yields [22]:

$$k\left.\frac{\partial T}{\partial Z}\right|_{Top} = \frac{J_w}{J_w + J_T} q_1 \tag{17}$$

R_P and R_S represent the tool pin and shoulder radius, respectively and q1 represents the total rate of heat generation at the shoulder–workpiece interface. It is given by [22]:

$$q_1 = \left[\eta\left(1-\delta\right)\tau + \delta\mu_F P_H\right]\left(\omega r - U_1 \sin\theta\right) \tag{18}$$

At the bottom surface, there is a backing plate and the heat transfer coefficient from the bottom of the workpiece is not the same as for free convection. The value of the heat transfer at bottom of workpiece was determined by:

$$k\left.\frac{\partial T}{\partial Z}\right|_{Bottom} = h_b\left(T - T_a\right) \tag{19}$$

Where, h_b is the bottom heat transfer coefficient and Ta is the ambient temperature of 298 K. The heat transfer coefficient at the bottom face depends on the local temperature and is given by the following relation [24]:

$$h_b = h_{b0}\left(T - T_a\right)^{0.25} \tag{20}$$

Where, h_{b0} is the heat transfer parameter for the bottom surface. As Equation (20), shows this parameter is a constant and it has a different unit than the heat transfer coefficient which is spatially variable. At the top surface, heat transfer is due to both convection and radiation and is given by:

$$-k\left.\frac{\partial T}{\partial Z}\right|_{Top} = \mathrm{B}\epsilon\left(T^4 - T_a^4\right) + h_t\left(T - T_a\right) \tag{21}$$

B is the Stefan–Boltzmann constant (5.67×10^{-16} $J.K^{-4}.m^{-2}.s^{-1}$), ε is the emissivity and h_t is the convective heat transfer coefficient at the top surface. The computed temperature values were found to be insensitive to the values of ht and its value was taken as zero for simplicity. During the simulation, linear and rotational speed of the tool pin and shoulder were performed separately. For this purpose, the sum of the rotational and linear speeds as separate components in a Cartesian coordinate system was defined. Figure 1 shows detachment of linear and rotational speeds into a unified coordinate system.

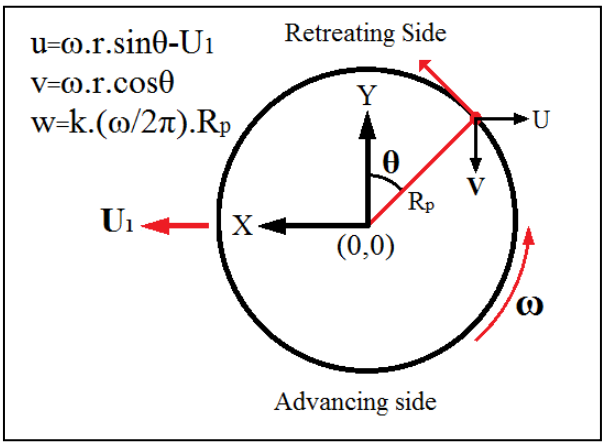

Figure1. Detachment of linear and rotational speeds

Velocities at the tool pin periphery have been defined in terms of tool translation velocity and the tool pin angular velocity [28]:

$$u = \left(\omega R_p \sin\theta - U_1\right) \tag{22}$$

$$v = \left(\omega R_p \cos\theta\right) \tag{23}$$

$$w = k\left(\frac{\omega}{2\pi}\right) R_P \tag{24}$$

K in Equation (24), represents the pitch on the pin tool. At all other surfaces, temperatures are set to ambient temperature (298 K).

2.2 Process Modeling and Mesh Generation

In this model a spherical pin with 0^o tilt angel was designed as FSW tool with 25.4 mm shoulder diameter. The diameter of pin was 15.7mm and pin height was 9.91mm. The base metal was assumed as non-Newtonian fluid with visco-plastic behaviour and density based on Ti-6Al-4V titanium alloy. The Tetrahedral/Hybrid elements with T-grid combination shape were used to the mesh generation of tool and workpiece. The region close to the pin tool and the tool itself required a much finer mesh to evaluate the heat transfer model and viscous flow. A sizing function on the tool and workpiece was used to generate the different volume sizes. The sizing function uses a start size, growth rate and maximum size. For the fine mesh pictured in Figure 2, a start size was 0.1 mm, growth rate 1.3 mm, and a maximum size of 1.5 mm. For this meshing scheme, the total number of volumes for the lateral case was 3,864,200 volumes.

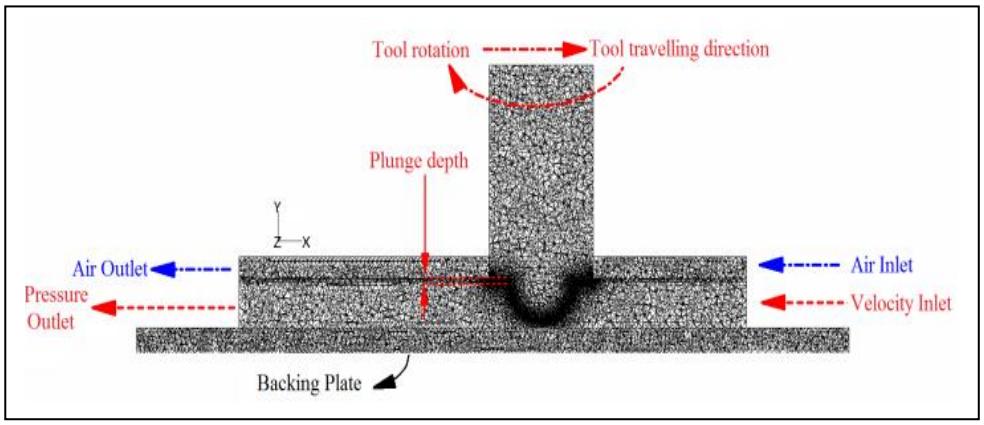

Figure2. Meshed model of the process

3. Experimental Procedure

The simulation results were validated by Pilchack et. al. experimental tests [29-31]. They used 10.3-mm-thick Ti-6Al-4V plates in the mill-annealed condition. Pilchack et. al. used a W-1 pct La2O3 tool with 25-mm-diameter and a simple 9.9mm long rounded probe. The used welding parameters by Pilchack et. al. were 120, 150, 200, 400 and 800 rpm rotational speed and 50, 101 and 203 mm/min travelling speed with 0^o tilt angle and constant plunge depth (0.025mm).In-tool temperature measurements were made using K-type thermocouples that were placed at two points along the centreline of the welding tool, as indicated in Figure 3, by spot welding the thermocouple into 3 mm diameter holes drilled in the tool. Thermocouple 1 (T1) was at shoulder level, while thermocouple 2 (T2) was 12.7 mm above T1. A HOBO (Onset, Bourne, MA) data logger was used to record temperature measurements at a rate of 1 Hz during welding.

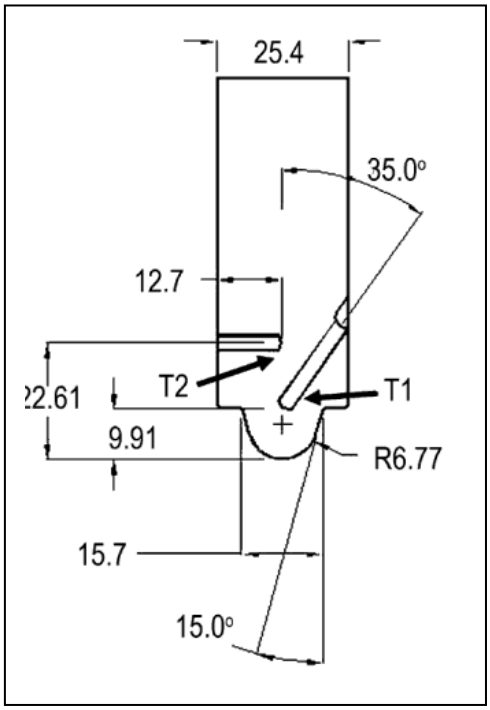

Figure3. FSW tool and K- thermocouples [29]

4. Results and Discussions

4.1 Heat Generation Rate

The term of heat generation rate in this study is ratio of the total generated heat by each part of tool in the different rotational speed, linear velocity, tool offset and tool tilt angle [32-33]. It can be concluded that the rate of heat production in each part of the tool depends on the extent of the contact area with the workpiece. The result shows that, the maximum heat amount generated in the exterior portion of the shoulder is 1000 degrees Kelvin in 800rpm and 50mm/min tool speed. The amount of heat is equal to 87% of the melting temperature of the titanium base metal. This heat is produced after 20s after tool transverse move. In lower tool rotational speed and higher tool travelling speed, the portion of frictional heat to melting temperature of titanium is decreased. Generally, it can be concluded that the maximum heat generated in this process is created by the tool shoulder and it is due to the greater contact area between tool shoulder with and the workpieces. With increasing rotational speed more frictional heat generates and with increasing tool traverses speed, the amount of heat generating decreases. The maximum heat generated in this study was achieved at the 800 rpm rotational speed and 50mm /min linear velocity and the lowest heat is generated at the 120 rpm rotational speed and 203 mm/min linear velocity, respectively.

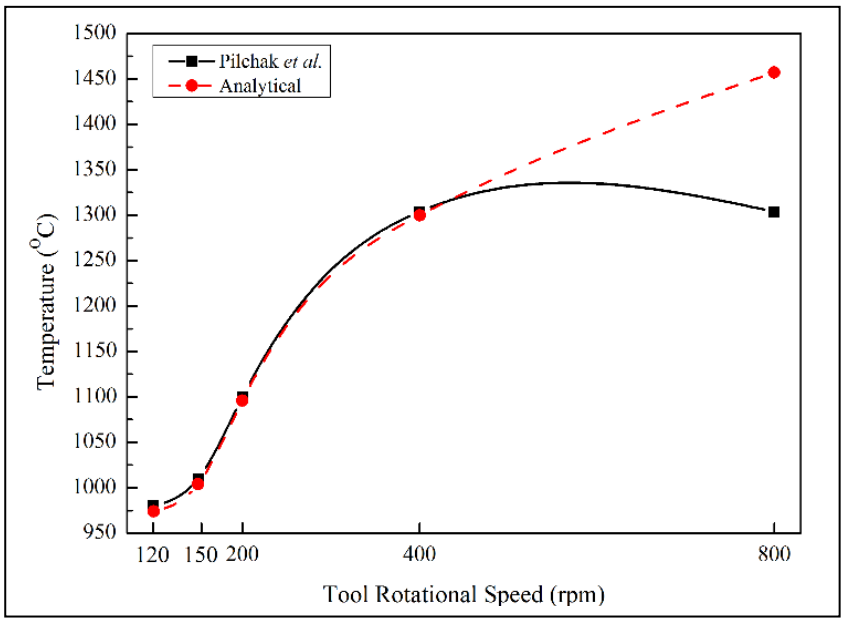

Figure4. Heat generated in different rotational and linear speeds

Based on results, the maximum heat that generated with tool shoulder is almost 3 times bigger than pin in joints. The comparison between numerical simulation and experimental maximum heat generated in various tool speeds are shown in Figure 4. The used thermocouple in Pilchak et. al. study was not able to record the heat generation in 800 rpm rotational speed [29],but the analytical study in FSW of Ti-6Al-4V material, predicted 1750K as maximum temperature in 800 rpm rotational speed. The main factor in formation of stir zone (SZ) FSW joint is heat generation which is dependent on the FSW tool parameters and flow of stirred materials. Figure 5presents simulation results of frictional heat generation from the start stage of process until reach to maximum

temperature. Because the chosen tool direction was CCW, the temperature diffusion on the advancing side (AS) was more than retreating side (RS). The results showed that the temperature distribution starts from the upper area of the joint. Due to more heat generation with the shoulder compared to other parts of the tool, heat diffusion into the work piece starts from the upper area of sheet.

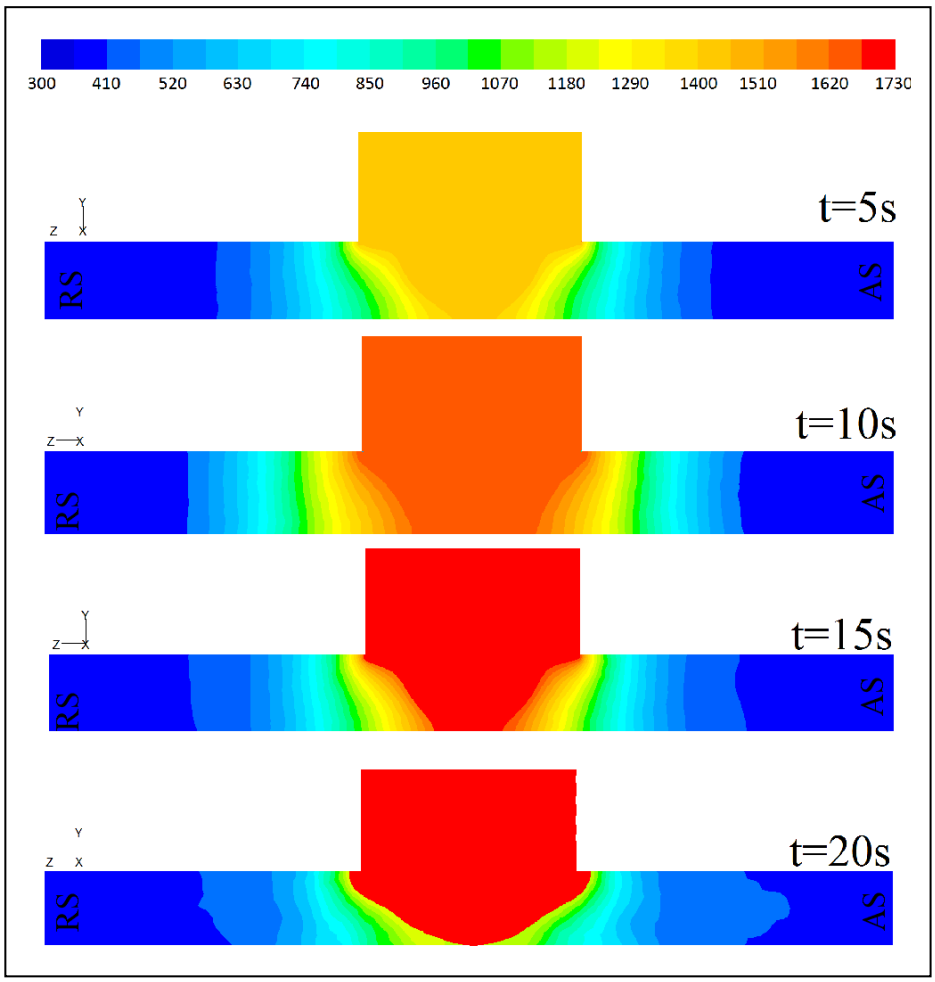

Figure5. Heat generated by the tool after (a) 5s, (b) 10s and (c) 20s welding start (the results are based on Kelvin degrees)

4.2 Heat Distribution

Figure 6 shows the simulation results of heat distribution that were produced by the various rotational speeds on the top surface of the workpiece. As can be seen, due to the tool rotation direction, heat distribution in the advancing side was more than retreating side in all cases. The CCW tool rotation direction leads the heat from retreating side to the advancing side in all cases. This phenomenon is consequence of material flow that accrues during FSW tool stirring. The being of the high temperature in the surrounding area of the tool was caused by the plastic deformation and friction as a result of high strain rate close to the FSW tool. The temperature gradient was much steeper in front of the tool than behind the tool.

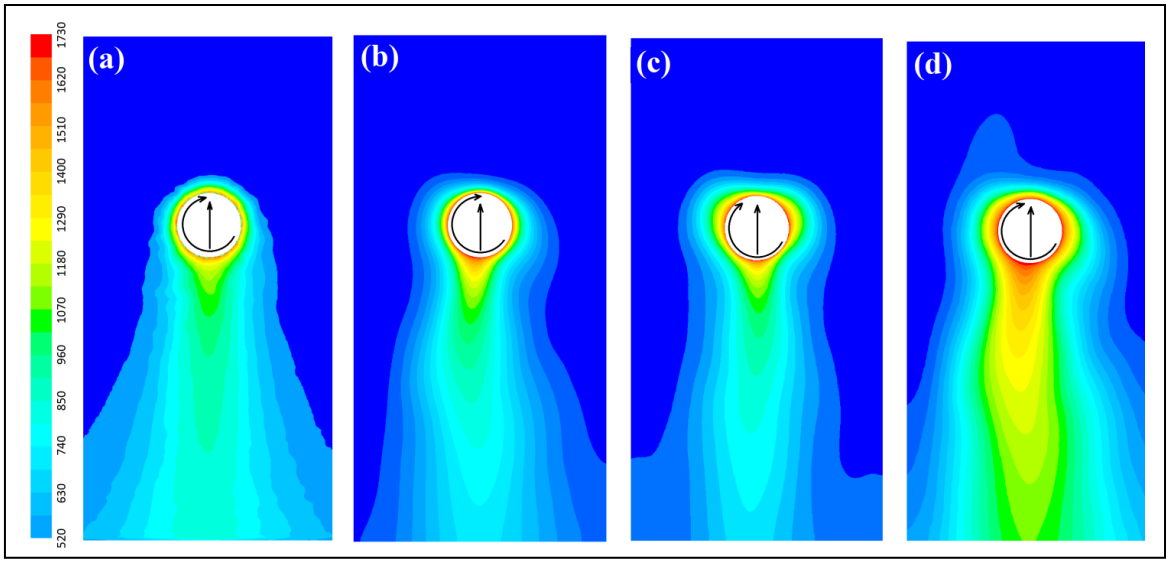

Figure6. Heat distribution at top surface of workpiece which welded with 50mm/min and (a) 120, (b) 200, (c) 400 and (d) 800 rpm tool speed

This phenomenon is a result of lower heat flux in front of tool compared to tool back. As seen in the Figure 6(a) and 6(b), at the 120 and 200rpm tool rotational speed and 50mm/min travelling speed, heat diffusion in surface of Ti-6Al-4V is not a comprehensive compare to joints which are welded with higher tool rotational speed. This is result of low frictional heat which was generated at low rotational speed and it is followed by more cooling rate. With increasing tool rotation till 400 and 800rpm, the heat was generated in the SZ growth up and heat affected area in top surface of workpiece became more. The heat distribution in top surface of joints which welded with 400 and 800rpm and 50mm/min travelling speed are shown in Figures 6(c) and 6(d), respectively.

4.3 Formation of Stir Zone

The material flow in FSW area showed four distinct regions that can be identified in the cross section, namely, the stir zone (SZ), thermo-mechanical zone (TZ), heat affected zone (HAZ), and base metal (BM) which are shown in Figure 7. The macrostructure of Ti-6Al-4V weld was bowl shaped and relatively featureless at the macroscopic scale with no bands or onion pattern evident.

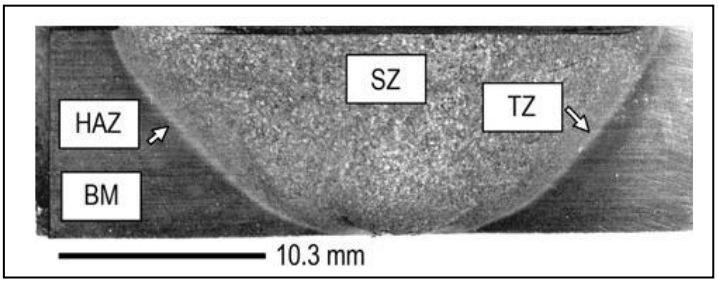

Figure7. Cross section view of Ti-6Al-4V joint [29]

Figure 8 shows the simulation result and actual material flow around pin in 800 rpm tool rotational speed and 50 mm/min travelling speed. In parameters, the frictional heat reached the highest

temperature, a banded structure in stir zone was observed. However, in the experimental study, energy dispersive spectroscopy revealed that the band contrast was due to the presence of tungsten in solid solution, leading to local elevation of the average atomic number [29-31]. Similarly the material flow around tool in the simulation results, the bands began at approximately the central stir zone and extended to the advancing side, where they all joined and formed one narrow line corresponding to the periphery of the pin. Figure 8 (a) shows the stream lines bands were wider near the central stir zone due to simulation result. In the lower magnification images of the Ti-6Al-4V bands in stir zone. Figure 8(b) shows the advancing side contrast gradients indicate which indicate chaotic flow patterns with folds and kinks that result in material apparently travelling backward in some locations. These features may be evidence for the occurrence of the ‘‘slip-stick’’ phenomenon that has been described to occur at the tool/workpiece interface [29-31].The banded structure shape which formed around tool pin is visible in Figure 8(c). These bands were widespread near the stir zone, where the tool traverse and the rotational velocity are orthogonal and parallel on the advancing side. In the lower magnification images of these bands, the differences related with the titanium-rich and tungsten-rich areas within the bands provide a qualitative indication of material flow behaviour directly at the tool/workpiece interface which is shown in Figure 8(d).

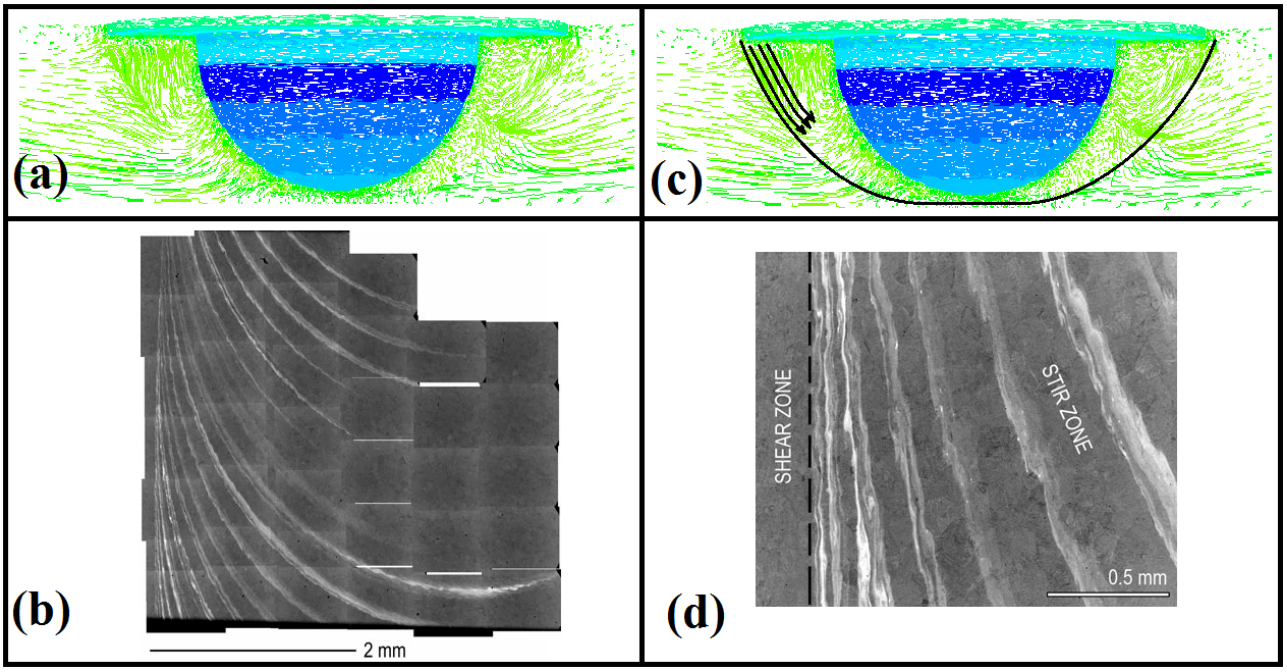

Figure8. (a) Simulation result, (b) actual material flow in stir zone [29], (c) Stream lines direction and (d) titanium band structure in stir zone [29]

4.4 Study of Torque

Figure 9(a) shows a comparison between the computed and the experimentally determined torque for various tool rotational speeds. As can be seen, there is good agreement between the simulation result and the experimental results of torque as affected by the tool rotation speed. The torque is relatively sensitive to the tool rotation speed because the change in the tool rotational speed does affect the computed temperature field around the tool pin. The results show that with increasing tool

rotation, torque decreases at constant tool travelling speed, due to two contributing factors. Firstly, for a constant welding speed and increasing tool rotation rate, the volume of material being deformed on each revolution increases, hence the heat is generated in a bigger volume, and this in turn may lead to slightly higher temperatures and lower flow stress. Secondly, higher tool rotation speeds will reduce the convective cooling. On the other hand, the torque is relatively insensitive to the welding speed because the change in the welding speed does not affect the computed temperature field around the tool pin as much as the tool rotation rate. For a constant tool rotation rate and decreasing welding speed, the volume of material being deformed on each revolution decreases, hence the heat is generated in a smaller volume, and this in turn may lead to slightly higher temperatures and lower flow stress. Lower welding speeds will reduce the convective cooling, resulting from slower movement into the relatively cooler material in front of the tool. Figure 9(b) shows the computed torque in different tool rotation and travelling speed.

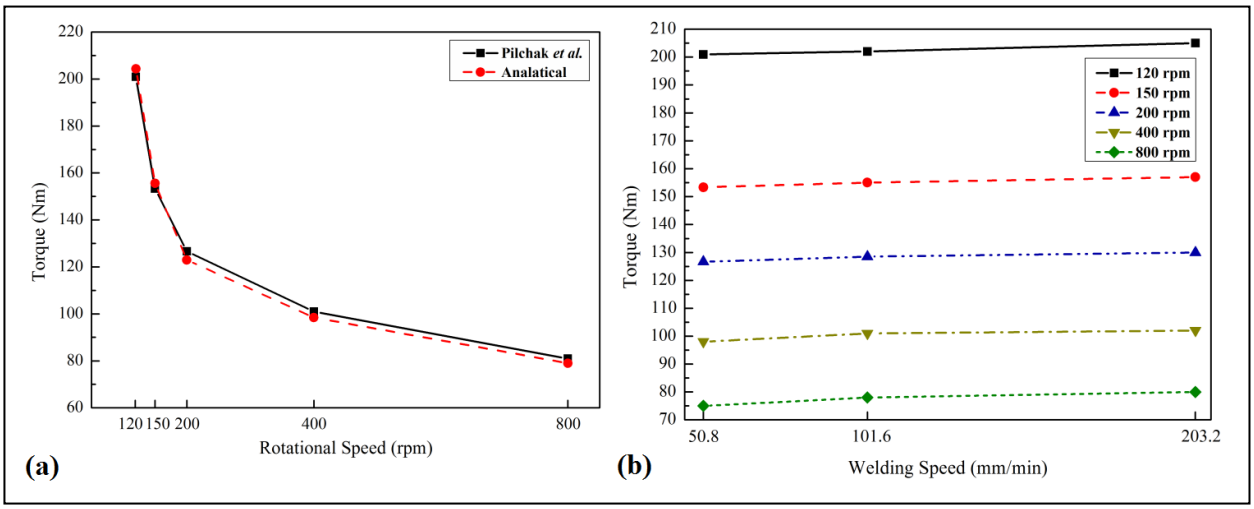

Figure9. (a) Comparison between the computed and the experimentally determined torque for various tool rotational speeds, (b) Comparison result between torque and welding speed

4.5 Study of Pressure and Strain Rate

Study of pressure is essential in the friction stir welding process simulation in order to obtain the material flow. A careful analysis of the pressure distribution could provide clues about the forging of the plasticized alloy behind the tool and the formation of defects in FSW [24]. Figure 10 shows the distribution of pressure in surface of Ti-6Al-4V welded at rotational speed of 800 rpm and welding velocity of 50 mm/min.

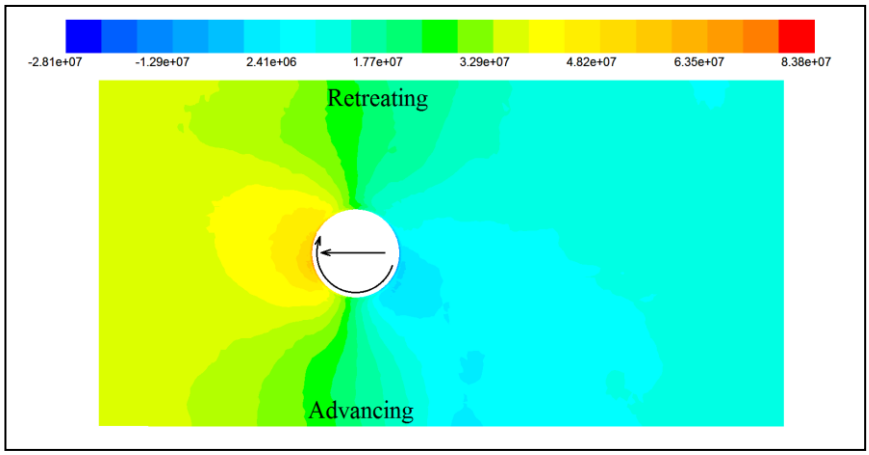

Figure10. Simulation result of pressure distribution on the top surface of workpiece

Pressure is higher in front of the tool as expected compared to the trailing edge. The pressure distribution is symmetric about the weld centerline due to symmetry in the velocity profile. Pressure is somewhat higher on the retreating side than the advancing side. They noted that material is not pressed against the tool at the back advancing side of the pin and this may be the region of void formation. The result shows that the maximum and minimum pressure in front and back of tool were predicted 0.635MPa and -0.28MPa, respectively. This result shows good flow ability of Ti-6Al-4V during FSW, due to the more forging force of materials from leading edge into trialing edge. Indeed this phenomenon indicates SZ fills with appropriate volume of material and possibility of defect formation decrease. Figure 11 shows strain-rate distribution in surface of welded titanium alloy.

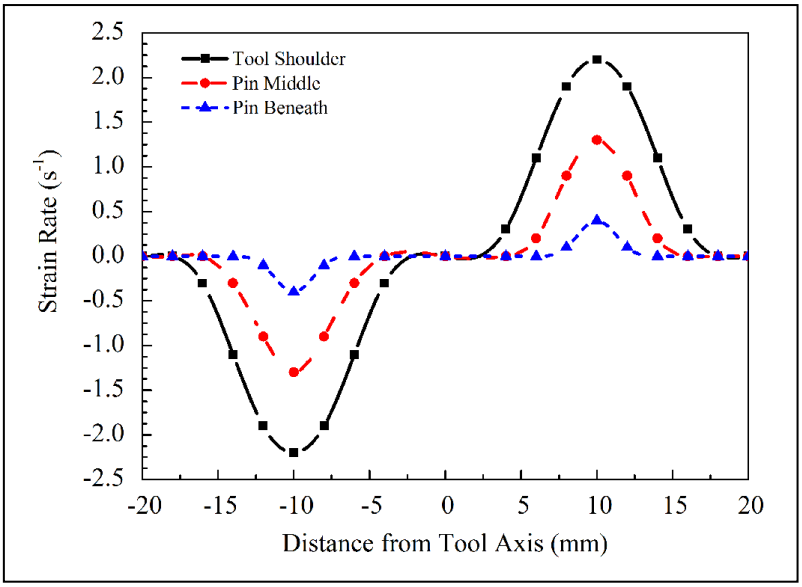

Figure11.Computed strain rate during FSW process

On average, strain-rates are higher at higher rotational speed, as expected. Very low strain-rate is indicative of poor flow ability due to reduced plasticization. Insufficient flowing material may result in surface lack of flow, wormhole, or lack of consolidation defects on the advancing side [34]. On

the other hand, if rotational speed is very high defects like flash formation, surface galling and nugget collapse may occur [34]. The simulation result shows that the maximum strain rate was accrue in surface contact between tool shoulder and Ti-6Al-4V. The maximum strain sate in mentioned area was 2.3 s^{-1}, and in the middle of tool pin and tool pin beneath were 1.1s^{-1} and 0.4s^{-1}, respectively.

5. Conclusion

In this study, 3D CFD developed model of friction stir welding of Ti-6Al-4V alloy was simulated. The flow pattern, defect formation prediction and temperature distribution were assessed with different rotational and linear velocities. The simulation results are titled as follows:

1. The maximum frictional heat was generated by tool shoulder (near 85% of total heat), due to the more contact area with the workpiece. According to the selected parameters, the maximum temperature was produced at 800rpm tool rotational and 50mm/min travelling speed (1750 K), and the lowest temperature was produced at 120rpm rotational speed and 203 mm/min linear velocity (1250 K).
2. The formation of stir zone coincide with chaotic flow patterns with folds and kinks that result in material apparently travelling backward in stir zone caused formation of banded structure around tool pin.
3. The exerted torque on titanium alloy is relatively sensitive to the tool rotation speed, but torque is relatively insensitive to the welding speed because the change in the welding speed does not affect the computed temperature field around the tool pin as much as the tool rotation rate.
4. The pressure distribution is higher in front of the tool compared to the trailing edge.This behavior indicate SZ fills with appropriate volume of material and possibility of defect formation decrease. The pressure distribution is symmetric about the weld centreline due to symmetry in the velocity profile. Pressure is somewhat higher on the retreating side than the advancing side.
5. The simulation result shows that the maximum strain rate was in interface surface of tool shoulder and Ti-6Al-4V. The maximum strain sate in mentioned area was 2.3 s^{-1}, and in the middle of tool pin and tool pin beneath were 1.1 s^{-1} and 0.4 s^{-1}, respectively.

6. References

[1] Aghajani Derazkola, H., Habibnia, M. and Jamshidi Aval, H. 2015. Study on Frictional Heat Behavior and Material Flow during Friction Stir Welding of AA1100 Aluminum Alloy. Modares Mechanical Engineering. 14: 251-261.

[2] Elyasi, M., Aghajani Derazkola, H. and Hosseinzadeh, M. 2015. Effects of Friction Stir Welding Parameters on Mechanical Quality of AA1100 Aluminum Alloy to A441 AISI Steel Joint. Modares Mechanical Engineering. 15: 379-390.

[3] Aghajani Derazkola, H., Elyasi, M. and Hosseinzadeh, M. 2016. Effects of Friction Stir Welding Tool Plunge Depth on Microstructure and Texture Evolution of AA1100 to A441 AISI Joint. International Journal of Advanced Design and Manufacturing Technology. 9: 13-20.

[4] Aghajani Derazkola, H., Elyasi, M. and Hosseinzadeh, M. 2015. Formation of Defects and Intermetallic Compounds in Friction Stir Welding of AA1100 Alloy to A441 AISI Steel. Advanced Processes in Materials. 9(3): 219-233.

[5] Elyasi, M., Aghajanai Derazkola, H. and Hosseinzadeh, M. 2016. Investigations of Tool Tilt Angle on Properties Friction Stir Welding of A441 AISI to AA1100 Aluminium. Proceedings of the Institution of Mechanical Engineers, Part B: Journal of Engineering Manufacture. 230(7): 1234-1241.

[6] Aghajanai Derazkola, A. and Simchi, A. 2018. Effects of Alumina Nanoparticles on the Microstructure, Strength and Wear Resistance of Poly (Methyl Methacrylate)-based Nanocomposites Prepared by Friction Stir Processing. Journal of the Mechanical Behavior of Biomedical Materials. 79: 246-253.

[7] Elyasi, M., Aghajanai Derazkola, H. and Hosseinzadeh, M. 2015. Study on Joint Zone Microstructure Evolution and Hardness in Friction Stir Welding of AA1100 Aluminum Alloy to A441 AISI Steel. Modares Mechanical Engineering. 14: 97-107.

[8] Aghajani Derazkola, H., Elyasi, M. and Hosseinzadeh, M. 2014. Feasibility Study on Aluminum Alloys and A441 AISI Steel Joints by Friction Stir Welding. International Journal of Advanced Design and Manufacturing Technology. 7: 99-109.

[9] Mironov, S., Sato, S.Y. and Kokawa H. 2018. Friction-Stir Welding and Processing of Ti-6Al-4V Titanium Alloy: A Review. Journal of Materials Science and Technology. 34(1): 58-72.

[10] Smith, C., Bendzsak, G., North, T., Hinrichs, J., Noruk, J. and Heideman, R. 1999. Heat and Material Flow Modeling of the Friction Stir Welding Process. 11th International Conference on Computer Technology in Welding, Detroit, United State.

[11] North, T., Bendzsak, G. and Smith, C. 2000. Material Properties Relevant to 3-D Modeling. 2nd International Friction Stir Welding Symposium. Gothenburg, Sweden.

[12] Seidel, T. U. and Reynolds, A. P. 2003. Two-Dimensional Friction Stir Welding Process Model based on Fluid Mechanics. Science and Technology of Welding and Joining. 8: 175-183.

[13] Zhang, W., DebRoy, T., Palmer, T. A. and Elmer, J. W. 2005. Modeling of Ferrite Formation in a Duplex Stainless Steel Weld Considering Non-Uniform Starting Microstructure. Acta Materialia. 53: 4441–4453.

[14] Nandan, R., Roy, G. and DebRoy, T. 2006. Numerical Simulation of Three Dimensional Heat Transfer and Plastic Flow During Friction Stir Welding. Metallurgical and Materials Transactions A. 37: 1247–1259.

[15] Nandan, R., Roy, G., Lienert, T. and DebRoy, T. 2006. Numerical Modelling of 3D Plastic Flow and Heat Transfer During Friction Stir Welding of Stainless Steel. Science and Technology of Welding and Joining. 11: 526-537.

[16] Nassar, H. W. and Khraisheh, M. K. 2012. Simulation of Material Flow and Heat Evolution in Friction Stir Processing Incorporating Melting. Journal of Engineering Materials and Technology. 134: 61-67.

[17] Ji, S.D., Shi, Q. Y., Zhang, L. G., Zou, A. L., Gao, S. S. and Zan, L. V. 2012. Numerical Simulation of Material Flow Behavior of Friction Stir Welding Influenced by Rotational Tool Geometry. Computational Materials Science. 63: 218–226.

[18] Aghajanai Derazkola, H. and Simchi, A. 2018. Experimental and Thermomechanical Analysis of Friction Stir Welding of Poly(Methyl Methacrylate) Sheets. Science and Technology of Welding and Joining. 23(3): 209-218.

[19] Elyasi, M. and Aghajanai Derazkola, H. 2018. Experimental and Thermomechanical Study on FSW of PMMA Polymer T-joint. The International Journal of Advanced Manufacturing Technology. https://doi.org/10.1007/s00170-018-1847-7.

[20] Kishore, VR. Arun, J., Padmanabhan, R. and Balasubramanian, V. 2015. Parametric Studies of Dissimilar Friction Stir Welding Using Computational Fluid Dynamics. The International Journal of Advanced Manufacturing Technology. 80(1–4): 91–98.

[21] Padmanaban, R., Kishore, V. R. and Balusamy, V. 2014. Numerical Simulation of Temperature Distribution and Material Flow During Friction Stir Welding of Dissimilar Aluminum Alloys. Procedia Engineering. 97: 854–863.

[22] Chen, G. 2017. Computational Fluid Dynamics Modeling on Steady-State Friction Stir Welding of Aluminum Alloy 6061 to TRIP Steel. Journal of Manufacturing Science and Engineering. 139: 1–12.

[23] Aghajani Derazkola, H., Elyasi, M. and Hosseinzadeh, M. 2015. CFD Modeling of Friction Stir Welding of AA1100 Aluminum Alloy to A441 AISI Steel Butt Joint. Journal of Advanced Materials and Processing. 3(3): 47–59.

[24] Aghajani Derazkola, H., Khodabakhshi, F. and Simchi, A. 2018. Friction-Stir Lap-Joining of Aluminium-Magnesium/Poly-methyl-methacrylate Hybrid Structures: Thermo-mechanical Modelling and Experimental Feasibility Study. Science and Technology of Welding and Joining. 23(1): 35-49.

[25] Jamshidi Aval, H., Serajzadeh, S. and Kokabi, A. H. 2011. Thermo-mechanical and Microstructural Issues in Dissimilar Friction Stir Welding of AA5086-AA6061. Journal of Material Science. 46(10): 3258–3268.

[26] Davis, J. R. 1995. Nonferrous Alloys and Special-Purpose Material, Ohio: ASM Handbook.

[27] Brandes, E. A. and Brool, G. B., 2004. Smithells Metals Reference Book, 8th Edition, Oxford:Elsevier.

[28] Liechty, B. C. and Webb, B. W., 2008. Modeling the Frictional Boundary Condition in Friction Stir Welding. International Journal of Machine Tools and Manufacture. 48: 1474-1485.

[29] Pilchak, A. L., Tang, W., Sahiner, H., Reynolds, A. P. and Williams, J. C. 2011. Microstructure Evolution during Friction Stir Welding of Mill-Annealed Ti-6Al-4V. Metallurgical and Materials Transaction A. 42: 745-762.

[30] Pilchak, A. L. and Williams, J. C. 2001. Microstructure and Texture Evolution during Friction Stir Processing of Fully Lamellar Ti-6Al-4V", Metallurgical and Materials Transaction A. 42: 773-794.

[31] Pilchak, A. L., JUHAS, M.C. and Williams, J. C. 2007. Microstructural Changes Due to Friction Stir Processing of Investment-Cast Ti-6Al-4V. Metallurgical and Materials Transaction A. 38: 401-408.

[32] Aghajani Derazkola, H. 2017. Effects of tool linear and rotational speed on material flow and heat generation of poly methyl methacrylate (PMMA) friction stir welding. Journal of Simulation and Analysis of Novel Technologies in Mechanical Engineering. 4: 687-700.

[33] Aghajani Derazkola, Kashiry Fard, R., H. and Khodabakhshi, F. 2018. Effects of processing parameters on the characteristics of dissimilar friction-stir-welded joints between AA5058 aluminum alloy and PMMA polymer. Welding in the World. 62(1): 117-130.

[34] Arbegast, W. J. 2008. A Flow-partitioned Deformation Zone Model for Defect Formation during Friction Stir Welding. Scripta Materialia. 58: 372-376.